Materials Research Bulletin 47 (2012) 2227–2234

Contents lists available at SciVerse ScienceDirect

Materials Research Bulletin

journal homepage: www.elsevier.com/locate/matresbu

Synthesis, structural characterization and Mössbauer study of $LnV_{0.5}Fe_{0.5}O_3$ perovskites (Ln = Y, La, Ce, Pr, Nd, Sm, Eu, Gd, Tb, Dy, Ho and Er)

Flávio F. Ivashita [a], Valdecir Biondo [a], Jusmar V. Bellini [a], Andrea Paesano Jr.[a], M. Cecilia Blanco [b], Valeria C. Fuertes [b], Elisa V. Pannunzio-Miner [b,1], Raúl E. Carbonio [b,1,*]

[a] Departamento de Física, Universidade Estadual de Maringá, Av. Colombo 5790, 87.020-900 Maringá, PR, Brazil
[b] INFIQC-CONICET, Departamento de Fisicoquímica, Facultad de Ciencias Químicas, Universidad Nacional de Córdoba, X5000HUA Córdoba, Argentina

ARTICLE INFO

Article history:
Received 17 December 2011
Received in revised form 18 May 2012
Accepted 30 May 2012
Available online 9 June 2012

Keywords:
A. Inorganic compounds
A. Oxides
C. Mössbauer spectroscopy
C. X-ray diffraction

ABSTRACT

Perovskites $LnV_{0.5}Fe_{0.5}O_3$ (Ln = Y, La, Ce, Pr, Nd, Sm, Eu, Gd, Tb, Dy, Ho and Er) were synthesized by rapid solidification from arc-melted samples and characterized by the study of their crystal structure and hyperfine properties. These metastable solid solutions crystallized in the *Pbnm* symmetry, with the iron and vanadium cations randomly distributed in the transition metal octahedral sites. Depending on the lanthanide present at the A site of the perovskite, iron is present with two valences (i.e., Fe^{3+} and Fe^{2+}). The volume of the unit cell for these perovskites increases linearly with the lanthanide ionic radius, as the perovskite approaches its ideal structure. At room temperature, the quadrupolar splitting of the trivalent paramagnetic Mössbauer component works as an indirect measurement for the Goldshmidt tolerance factor. Close to or below 100 K, these perovskites undergo a crystallographic phase transformation, probably due to orbital ordering of the V^{3+} cations, originating two different magnetic iron sites.

1. Introduction

Perovskites are oxides with ideal formula ABO_3, where A is a divalent cation (e.g., Ca^{2+}, Sr^{2+}, Ba^{2+}) or a trivalent cation such as Bi^{3+}, Ln^{3+} or Y^{3+}. B is, in general, a trivalent or tetravalent transition metal cation. Among those with $A = Ln^{3+}$, manganites (B = Mn), orthoferrites (B = Fe) and orthovanadates (B = V) constitute important subfamilies of perovskites and have been extensively studied because of their intriguing fundamental properties and technological importance.

The orthoferrites ($LnFeO_3$) were first synthesized in the 1940s [1] and since then they have been characterized practically by every known experimental technique applicable to solid systems. Their structural properties, phase transitions, electric and magnetic properties, in particular, were deeply explored because they match technological applications such as membranes for gas separators, cathodes in solid oxide fuel cells, catalysts, sensor materials, gas sensors, magneto optical materials and spin-valves [2–9].

By the mid 1950s, solid state researchers also turned their attention to the $LnVO_3$ compounds, which exhibit a wide variety of interesting physical properties, among which the orbital ordering is the most striking one [10,11]. More recently, manganites have received a lot of attention because of their colossal magnetoresistance [12,13].

It is possible to explore new applications for these compounds synthesizing them through chemical substitutions at the A and B sites provided, of course, that the ionic radius and charge neutrality criteria are satisfied. Indeed, a number of combinations – either at A site (with two or more lanthanides) or at B site (with two or more transition metals) – were examined and novel or unusual physical properties were discovered, such as the half-metallic antiferromagnetism [14] and metal-insulator transitions [15].

In spite of the very interesting effects that could plausibly also be expected from the iron doping of the orthovanadates or, alternatively, from the vanadium doping of orthoferrites, only few studies were previously reported on $LnV_{1-x}Fe_xO_3$ perovskites [16,17]. Some difficulties are on account of the question of the simultaneous stabilization of a reduced V^{3+} cation with the oxidized Fe^{3+} cation. In fact, Gateshki et al. [17] reported that several heat-treatments at 1400 °C and regrindings were necessary to obtain $RFe_{0.5}V_{0.5}O_3$ (R = Y, Eu, Nd, La), which always contain small amounts of RVO_4.

Moreover, motivated by the new physical properties that such compounds could potentially present, we started an extensive study on this perovskite family, with most of the lanthanides and Y that we baptized as orthoferrivanadates.

In this paper, we report crystallographic and Mössbauer spectroscopy data on the $LnV_{0.5}Fe_{0.5}O_3$ (Ln = Y, La, Ce, Pr, Nd, Sm, Eu, Gd, Tb, Dy, Ho and Er) orthoferrivanadates, synthesized for

* Corresponding author. Tel.: +54 351 433 4180; fax: +54 351 433 4188.
E-mail address: carbonio@fcq.unc.edu.ar (R.E. Carbonio).
[1] Members of the Research Career of CONICET.

0025-5408/$ – see front matter © 2012 Elsevier Ltd. All rights reserved.
http://dx.doi.org/10.1016/j.materresbull.2012.05.055

most of the lanthanides and yttrium, by quenching from the liquid ceramic phase obtained from arc-melted samples.

2. Experimental methods

$LnV_{0.5}Fe_{0.5}O_3$ samples (for Ln = La, Ce, Pr, Nd, Sm, Eu, Gd, Tb, Dy, Y, Ho and Er) were prepared, first, by mixing Ln_2O_3, Fe_2O_3 and V_2O_3 powders (99.9% pure) in the prescribed molar ratio. This pre-mixture (~1 g) was pressed and arc-melted – at least three times – under argon atmosphere. The overall concentration was carefully checked, by weighting the samples before and after each stage of the synthesis (i.e., powder mixture ⇒ pressed cylinders of compacted powder, before melting ⇒ as-melted sample). The final as-melted button was then ground and sieved at 150 mesh. The powder was annealed under argon atmosphere for 12 h at 1100 °C. Additionally, in order to verify the inability of conventional methods to produce these metastable compounds, some samples were prepared by conventional ceramic process, i.e., the starting mixture was annealed in argon atmosphere and also powdered and sieved. A couple of end solid-solutions samples (i.e., $LnVO_3$ and $LnFeO_3$) were also prepared by either of the processes.

The compounds were structurally and hyperfine characterized by powder X-ray diffraction (PXRD) and Mössbauer spectroscopy (MS).

The characterization by PXRD was done using a conventional diffractometer, in Bragg–Brentano reflection geometry, with Cu Kα radiation (λ = 1.5418 Å). The data were obtained between 15° and 120° (2θ), in steps of 0.02° and 10 s per step. The diffractograms were refined by the Rietveld method, using the FULLPROF program [18]. Zero shift, background, isotropic temperature factors, atomic positions, cell and profile parameters were refined using a pseudo-Voigt function.

Mössbauer spectra were taken from a constant acceleration spectrometer, with a $^{57}Co(Rh)$ source of 25 mCi of nominal starting activity. For the low temperature Mössbauer measurements, a helium/nitrogen flow cryostat was employed. The Mössbauer spectra were analyzed using a non-linear least-square routine, with Lorentzian line shapes. Eventually, a hyperfine magnetic field distribution, B_{hf} Dist., was used as histograms in the spectral analysis. All isomer shift (IS) data are given relative to α-Fe throughout this paper.

3. Results and discussion

3.1. Powder X-ray diffraction results

The refined diffractograms obtained for two representatives $LnV_{0.5}Fe_{0.5}O_3$ compounds (a light and a heavy rare earth element) are shown in Fig. 1. Table 1 lists the Rietveld refined parameters for all samples prepared in the present study.

The refined diffractograms revealed that all compounds were well refined with orthorhombic symmetry, in the *Pbnm* space group (Fig. 1), as usual for $LnBO_3$ perovskites. *R* factors are unusually high probably because of the crystallite strain produced by rapid solidification of the samples. As an example of this, Rietveld refinements of Ceria powders synthesized by high energy ball milling with large strain values give high R_{wp} values [19].

No peaks could be detected as a consequence of order among iron and vanadium in the B site, in which case a double perovskite would be generated. Actually, if we consider that the oxidation states for iron and vanadium sharing the same octahedral site (4b) are V^{3+} and Fe^{3+}, they do not meet the criteria of difference in ionic radii (i.r.) and valences for the double perovskite crystallization [20]. In fact, the results of the phenomenological Brown's Bond Valence Model [21] can give us an estimation of the actual valences of the cations and anions in the structure. The results are shown in Table 2. For the cations in the octahedral sites the average value is given. There is a very good agreement between these results and the nominal oxidation states of the different ions in the structure, confirming thus the assumption of 3+ oxidation states for vanadium and iron in the octahedral sites.

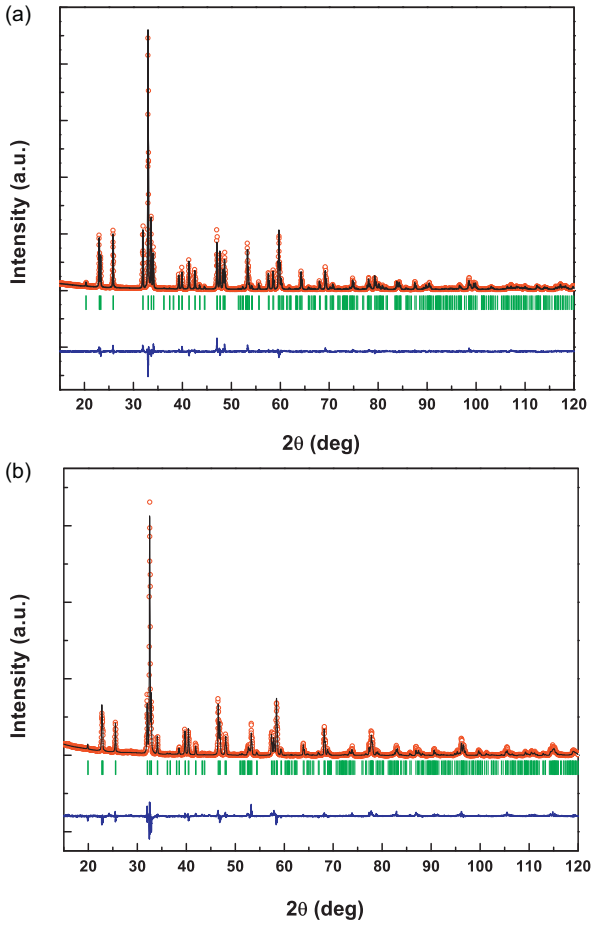

Fig. 1. Refined diffractograms for the $TbFe_{0.5}V_{0.5}O_3$ (a) and $NdFe_{0.5}V_{0.5}O_3$ (b) samples; circles = experimental data; line = calculated data; bottom (blue) solid line = difference between profiles; vertical bars represent positions of Bragg reflections. (For interpretation of the references to color in this figure legend, the reader is referred to the web version of this article.)

It is worthy saying that the formation of $LnFeO_3$ and $LnVO_4$ phases was observed by PXRD (not shown) when the pre-mixture was just annealed in any atmosphere at 1100 °C (i.e., without arc-melting), which indicates that the conditions established by the arc-melting synthesis are crucial in stabilizing these metastable orthoferrivanadates. In fact, recently Gateshki et al. [17], informed the synthesis of $LnFe_{0.5}V_{0.5}O_3$ (with Ln = Y, Eu, Nd or La) by several heat treatments at 1350 °C with intermediate regrindings, and even after the last heat treatment most of the compounds showed the presence of RVO_3 impurities (in the order of 1–2%). Under our conditions (arc-melting in Ar atmosphere) as confirmed by the Mössbauer results (presented ahead), a very small amount of α-Fe (<1 mol%) was detected from PXRD refinements for the Ln = Nd, Sm, Eu and Gd samples (for simplification, not considered in the $NdV_{0.5}Fe_{0.5}O_3$ refined diffractogram of Fig. 1). However, in spite of some other possible small impurities, no residual metallic iron could be verified for the samples with Ln = La, Ce, Tb, Dy, Ho and Er. The presence of the larger lanthanum and cerium ions on this list rules out any presumable simple dependence on the ionic radius of the rare-earth. Henceforth, these two groups of samples will be designated throughout this paper as Series I (Pr, Nd, etc.) and Series II (La, Ce, etc.).

Table 1
Crystallographic refined parameters, as obtained from the Rietveld analysis of laboratory PXRD data for $LnFe_{0.5}V_{0.5}O_3$ (Ln = Y, La, Ce, Pr, Nd, Sm, Eu, Gd, Tb, Dy, Ho and Er).

Ln in $LnV_{0.5}Fe_{0.5}O_3$	Phase purity (%)	Cell parameters (Å)	Atom site	Factional cell coordinates			Biso ($\times 100\,A^2$)	R_{Bragg}	R_{wp}	χ^2
La	96.4	5.5531(1)	La	0.99458(4)	0.03193(2)	0.25	0.096(2)	9.25	18.3	6.76
		5.5615(1)	V/Fe	0	0.5	0	0.374			
		7.8523(1)	O1	0.0617(5)	0.4978(2)	0.25	0.618			
			O1	0.7149(3)	0.2719(3)	0.0387(2)	0.142			
Ce	100	5.5199(4)	Ce	0.9968(1)	0.03754(3)	0.25	0.068(7)	10.1	26.0	2.71
		5.5674(4)	V/Fe	0	0.5	0	0.374			
		7.8152(5)	O1	0.0786(6)	0.4943(4)	0.25	0.618			
			O2	0.7134(4)	0.2982(4)	0.0426(3)	0.142			
Pr	>99	5.4866(4)	Pr	0.9905(1)	0.04577(4)	0.25	−0.331(8)	10.6	25.2	2.30
		5.5786(4)	V/Fe	0	0.5	0	0.374			
		7.7839(6)	O1	0.0992(5)	0.4932(4)	0.25	0.618			
			O2	0.7050(3)	0.2879(3)	0.0244(3)	0.142			
Nd	>99	5.4506(1)	Nd	0.98945(4)	0.04880(2)	0.25	−0.311(2)	8.75	17.2	4.05
		5.5857(1)	V/Fe	0	0.5	0	0.374			
		7.7522(1)	O1	0.1106(3)	0.4775(2)	0.25	0.618			
			O2	0.7149(2)	0.2880(2)	0.0426(4)	0.142			
Sm	>99	5.3982(1)	Sm	0.98591(5)	0.05565(2)	0.25	−0.642(2)	7.73	18.3	2.61
		5.5997(1)	V/Fe	0	0.5	0	0.374			
		7.6969(2)	O1	0.1030(3)	0.4801(3)	0.25	0.618			
			O2	0.7039(2)	0.3040(2)	0.0454(2)	0.142			
Eu	>99	5.3730(1)	Eu	0.98448(3)	0.05904(3)	0.25	−0.732(2)	12.0	19.8	4.55
		5.6091(1)	V/Fe	0	0.5	0	0.374			
		7.6733(1)	O1	0.0952(3)	0.4806(3)	0.25	0.618			
			O2	0.7015(2)	0.3037(3)	0.0450(2)	0.142			
Gd	>99	5.3477(1)	Gd	0.98402(3)	0.06263(2)	0.25	−0.515(2)	12.4	22.5	4.41
		5.6157(1)	V/Fe	0	0.5	0	0.374			
		7.6544(1)	O1	0.0960(3)	0.4670(3)	0.25	0.618			
			O2	0.6923(2)	0.3039(2)	0.0529(1)	0.142			
Tb	100	5.3260(1)	Tb	0.98303(2)	0.06411(1)	0.25	0.084(1)	7.18	14.9	3.53
		5.6026(1)	V/Fe	0	0.5	0	0.374			
		7.6277(1)	O1	0.0922(2)	0.4780(2)	0.25	0.618			
			O2	0.6911(2)	0.3143(12)	0.0471(8)	0.142			
Dy	100	5.3024(1)	Dy	0.98295(2)	0.06760(2)	0.25	0.061(2)	10.5	20.6	3.86
		5.6014(1)	V/Fe	0	0.5	0	0.374			
		7.6087(1)	O1	0.1048(2)	0.4733(2)	0.25	0.618			
			O2	0.6860(2)	0.3133(2)	0.0493(1)	0.142			
Y	98.8	5.2803(1)	Y	0.98281(3)	0.06975(2)	0.25	−0.411(2)	14.8	25.4	10.2
		5.5979(1)	V/Fe	0	0.5	0	0.374			
		7.5886(2)	O1	0.1157(2)	0.4756(2)	0.25	0.618			
			O2	0.6971(1)	0.3305(1)	0.0517(1)	0.142			
Ho	100	5.2795(1)	Ho	0.98050(3)	0.06716(2)	0.25	0.322(3)	10.6	20.1	6.80
		5.5968(1)	V/Fe	0	0.5	0	0.374			
		7.5900(1)	O1	0.1114(2)	0.4519(2)	0.25	0.618			
			O2	0.6995(5)	0.3005(1)	0.0455(1)	0.142			
Er	96.4	5.2615(1)	Er	0.98055(3)	0.06937(2)	0.25	−0.106(3)	9.09	18.7	11.3
		5.5898(1)	V/Fe	0	0.5	0	0.374			
		7.5761(1)	O1	0.1139(2)	0.4537(2)	0.25	0.618			
			O2	0.6835(2)	0.3161(2)	0.0607(1)	0.142			

Table 2
Calculated bond valence sums (BVS) with the Brown's model.

Ln in $LnV_{0.5}Fe_{0.5}O_3$ compound	Bond valence sums			
	Ln	V/Fe	O1	O2
Y	3.062(3)	3.048(4)	2.105(3)	2.002(4)
La	2.948(3)	3.025(6)	2.014(4)	1.970(3)
Ce	3.025(8)	2.993(2)	2.046(6)	1.986(5)
Pr	3.064(5)	3.007(1)	2.195(7)	1.938(4)
Nd	3.015(4)	2.968(6)	2.141(4)	1.921(2)
Sm	2.907(3)	3.033(4)	2.131(2)	1.934(3)
Eu	2.865(5)	3.054(8)	2.063(4)	1.913(5)
Gd	2.979(2)	2.981(4)	2.110(2)	1.925(3)
Tb	2.784(2)	3.003(4)	2.028(1)	1.897(1)
Dy	2.721(3)	2.971(4)	2.008(2)	1.842(2)
Ho	2.893(7)	3.108(1)	2.128(4)	1.931(5)
Er	2.937(3)	2.919(4)	2.046(3)	1.886(2)

On the other hand, the lanthanide cation size effectively controls the cell parameter in such a way that *a* and *c* linearly increase with its ionic radius, whereas *b* is nearly constant, as shown in Fig. 2. This invariance of *b* with the lanthanide ionic radii was similarly observed by Gateshki et al. for $RFe_{0.5}V_{0.5}O_3$ (with R = Y, Eu, Nd, La) [17] and by other authors for RVO_3 [22,23]. Martínez-Lope et al. assigned this small variation of the *b* parameter as due to the tilting scheme $a^-a^-c^+$ of VO_6 octahedra in *Pbnm* space group, in which the distortion driven by the reduction of the size of the Ln^{3+} leaves *b* almost unchanged [23]. The same behavior was informed for $RFeO_3$ by Marezio et al. [24], in fact, plotting the cell parameters obtained for RVO_3, $RFeO_3$, $RFe_{0.5}V_{0.5}O_3$ (with R = Y, Eu, Nd, La) and our results, all values are the same within the experimental error (see Supplementary Information, Fig. S1). This is reasonable, since $^{VI}(rFe^{3+}(HS)) = 0.645$ Å and $^{VI}(rV^{3+}) = 0.640$ Å [25]. For Ln = Lanthanum, $a \approx b \approx c/\sqrt{2}$, and the lattice becomes

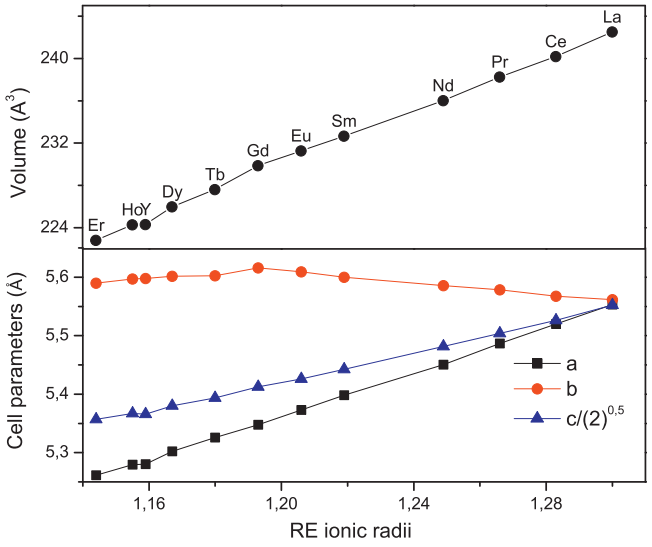

Fig. 2. Lattice parameters (a, b and $c/\sqrt{2}$) and cell volume vs. the Ln ionic radius for the $LnV_{0.5}Fe_{0.5}O_3$ samples.

pseudo-cubic. In fact, as the lanthanide decreases its size, the BO_6 octahedra are forced to tilt in order to decrease the distance Ln–O and the orthorhombic distortion increases. Tilt angles (Fe/V)–O1–(Fe/V) and (Fe/V)–O2–(Fe/V) and there average ⟨(Fe/V)–O–(Fe/V)⟩ are shown in Table 3. There is an increase in the average tilt angle as the lanthanide radii decreases, as expected. This was also observed by Martínez-Lope et al. for RVO_3 [23]. Bond distances are informed in Table 3. All average distances for eight coordination for Ln (A site) and six coordination for Fe/V (B site) are in very good agreement with the sum of ionic radii.

3.2. Mössbauer results

The fitted RT Mössbauer spectra for the $EuV_{0.5}Fe_{0.5}O_3$ and $DyV_{0.5}Fe_{0.5}O_3$ samples are shown in Fig. 3. The fitted hyperfine parameters for all compounds, including the values obtained by measurements at lower or higher temperatures, are listed in Table 4.

In both cases (Fig. 3a and b), one paramagnetic component is clearly visible in the central part of the spectra, in addition to a more complex magnetic fraction. Thus, all the spectra were fitted with, at least, a doublet (Fe^{3+}), plus a hyperfine magnetic field distribution and a discrete sextet, the latter eventually giving a very small or, even, a null contribution.

All these components may be attributed to magnetically different iron sites of the same perovskite phase. The fact that the B site is randomly occupied by Fe and V will produce different neighborhoods for the iron cations, i.e., Fe-rich ones with predominant Fe–O–Fe interactions, V-rich ones with predominant V–O–V interactions and mixed ones with predominant Fe–O–V interactions. It is expected that the Fe-rich ones will present antiferromagnetic regions like in the orthoferrites $LnFeO_3$, which will give place to the sextet in the Mössbauer spectrum. On the other hand, the mixed neighborhoods with predominant Fe–O–V interactions, where the antiferromagnetic order is weakened, will give place to a paramagnetic signal in the Mössbauer spectrum.

However, as pointed out above, $DyV_{0.5}Fe_{0.5}O_3$ and $EuV_{0.5}Fe_{0.5}O_3$ are representative cases of two different types of situations. Thus, for Series I, an additional discrete sextet – corresponding to α-Fe was included in the fitting process. The subspectral iron component reaches, at the maximum, about 8% which means that some orthoferrivanadates of Series I may have presented some deviation from their nominal composition. It is worth mentioning that this percentage is not representative of the mass percentage, since this was quantified by PXRD and it was found that at the maximum was 1%. The iron sextet was not found for Series II though another doublet (Fe^{2+}) appears in the spectra of this series. This was unexpected because the simplest cationic valence we could assign was $Ln^{3+}V^{3+}{}_{0.5}Fe^{3+}{}_{0.5}O^{2-}{}_3$, but for some reason iron occurs partially reduced (as Fe^{2+}) in Series II. Electronic equilibrium would require a compensating oxidation of the vanadium cation (i.e., V^{4+} or V^{5+}) or the introduction of anionic vacancies in the perovskite structure.

On the other hand, considering that the reduction of iron oxides by arc-melting is normally observed, vacancies formation would be the way the system finds to reach the local electronic neutrality. In principle, each oxygen vacancy implies the conversion of two trivalent iron cations into two divalent iron cations and, accordingly, the fraction of vacancies could be estimated to be – without considering the existence of V^{4+} or V^{5+} – one twelfth of the Fe^{2+} relative area, or less than that – do considering the existence of V^{4+} or V^{5+}. For the holmium orthoferrivanadate, which showed the largest Fe^{2+} population (see Table 2), the estimated fraction of oxygen vacancies is ~2.2%, i.e., absolutely within acceptable limits for perovskites [20].

The isomer shift of the trivalent paramagnetic component (i.e., the Doublet 1) varies slightly for the different orthoferrivanadates, whereas the quadrupole interaction increases for decreasing lanthanide ionic radius (i.r.).

It is interesting to plot QS superimposed the tilt angle along the a (or b) axis both as a function of the "Goldshmidt Tolerance Factor" (t) [20], as presented in Fig. 4. t should be ideally 1 for cubic perovskites, however, as the i.r. for the Ln cation decreases, t decreases, indicating that the perovskite is more distorted. As can be seen QS increases with decreasing t (i.e. increasing distortion). This discloses the quadrupolar splitting as an empirical indirect measure for the perovskite distortion. To the best of our knowledge, this correlation has not been shown for iron containing perovskites yet. As well, the correlation of QS with the tilt angle along the a (or b) axis shows an experimental correlation with the global distortion of the structure. In an attempt to correlate QS with local distortion of the FeO_6 octahedra we try to find correlations between distortion index and bond-angle variance index. The distortion index defined by Brown and Shannon [26] is a useful parameter to quantify distortions in polyhedra when no appreciable variation in bond angles occurs. It is defined as $\Delta = (1/n)\,10^3 \sum[(r_i - \langle r\rangle)/\langle r\rangle]^2$, where r_i is an individual bond length and $\langle r\rangle$ is the average bond length in the polyhedron. The bond-angle variance index (proposed by Robinson et al.) [27] is defined as $\delta = [1/(n-1)][\sum(\theta_i - \theta)^2]$, where θ_i represents the angle value calculated from the structure refinement and θ is the ideal angle for the polyhedron. We could not find any correlation between QS and the average distortion of the octahedra (Fe, V)O_6 (Δ) or bond-angle variance index (δ) (see Supplementary information, Fig. S2).

On the other hand, the behavior of the IS and QS for the divalent paramagnetic component (i.e., the Doublet 2) reveals no tendency, i.e., neither have any significant variations throughout the group. These IS values, particularly, are unusually small for divalent iron located at octahedral sites. They are more in the range of tetra- or penta-coordinated species. Nonetheless, other similar systems, e.g., FeTe/FeSe/FeS present comparable (or even smaller) IS values (i.e., 0.66 mm/s, 0.64 mm/s and 0.88 mm/s, respectively) [28]. This series of anions belonging to the Group VI A – including oxygen (Obs. IS_{FeO} = 1.20 mm/s) – presents increasing electronegativity from tellurium to oxygen (2.1, 2.4, 2.5 and 3.5, respectively). Based on this correlation, it is generally

Table 3
Selected bond distances, angles and tilt angles obtained after Rietveld refinements for $LnFe_{0.5}V_{0.5}O_3$ (Ln = Y, La, Ce, Pr, Nd, Sm, Eu, Gd, Tb, Dy, Ho and Er) and comparison of average bond distances with the sum of ionic radii.

Ln in $LnV_{0.5}Fe_{0.5}O_3$ compound	O–RE distances (Å)	O–RE average distance (Å)	O–RE ionic radii sum (Å)[a]	O–(Fe/V) distances (Å)	O–(Fe/V) average distance(Å)[b]	O–(Fe/V)–O angles (°)	(Fe/V)–O2–(Fe/V) tilt angles (°)	(Fe/V)–O1–(Fe/V) tilt angles (°)	⟨(Fe/V)–O–(Fe/V)⟩ tilt angles (°)
La	2.617(1) 2.471(2) 2 × 2.636(2) 2 × 2.489(2) 2 × 2.798(2)	2.617	2.560	2 × 1.9978(3) 2 × 1.9005(7) 2 × 2.1587(7)	2.028	2 × 90.27 2 × 90.85 2 × 91.23	11.5	11.5	11.5
Ce	2.583(2) 2.357(3) 2 × 2.738(2) 2 × 2.680(2) 2 × 2.398(2)	2.572	2.543	2 × 2.0015(7) 2 × 1.969(2) 2 × 2.063(2)	2.011	2 × 90.51 2 × 90.61 2 × 91.4	13.5	13	13.25
Pr	2.566(2) 2.269(3) 2 × 2.510(2) 2 × 2.609(2) 2 × 2.713(2)	2.562	2.526	2 × 2.0205(7) 2 × 2.013(2) 2 × 1.969(2)	2.001	2 × 96.79 2 × 94.56 2 × 90.41	11.5	17	14.25
Nd	2.484(1) 2.216(1) 2 × 2.439(1) 2 × 2.7362(9) 2 × 2.571(1)	2.524	2.509	2 × 2.0335(3) 2 × 1.9816(10) 2 × 2.0170(10)	2.010	2 × 90.93 2 × 93.79 2 × 90.41	13	17.5	15.25
Sm	2.459(1) 2.259(1) 2 × 2.595(1) 2 × 2.678(1) 2 × 2.349(1)	2.495	2.479	2 × 2.0060(3) 2 × 1.9701(1) 2 × 2.0571(1)	2.011	2 × 90.7 2 × 92.11 2 × 90.18	14	16.5	15.25
Eu	2.438(1) 2.301(1) 2 × 2.350(1) 2 × 2.660(1) 2 × 2.583(1)	2.490	2.466	2 × 1.9883(3) 2 × 1.976(1) 2 × 2.048(1)	2.004	2 × 90.88 2 × 90.48 2 × 90.49	15	15	15
Gd	2.348(1) 2.309(1) 2 × 2.297(1) 2 × 2.6794(9) 2 × 2.5581(9)	2.466	2.453	2 × 1.9899(3) 2 × 2.0209(9) 2 × 2.0333(1)	2.015	2 × 90.96 2 × 91.67 2 × 90.57	16	16.5	16.25
Tb	2.3907(8) 2.3131(8) 2 × 2.2840(6) 2 × 2.6128(6) 2 × 2.6033(6)	2.463	2.440	2 × 1.9730(2) 2 × 1.9793(6) 2 × 2.0652(6)	2.006	2 × 90.07 2 × 90.5 2 × 90.41	17	14.5	15.75
Dy	2.3625(11) 2.2488(11) 2 × 2.2725(8) 2 × 2.6059(8) 2 × 2.5892(8)	2.443	2.427	2 × 1.9873(3) 2 × 2.0016(8) 2 × 2.0477(8)	2.012	2 × 90.56 2 × 91.23 2 × 90.57	18	16.5	17.25
Y	2.378(1) 2.185(1) 2 × 2.5826(7) 2 × 2.6143(7) 2 × 2.2274(7)	2.426	2.419	2 × 1.9978(3) 2 × 1.9005(7) 2 × 2.1587(7)	2.019	2 × 91.55 2 × 92.11 2 × 91.05	19.5	19	19.25
Ho	2.2614(11) 2.2493(10) 2 × 2.3537(8) 2 × 2.6298(8) 2 × 2.5130(8)	2.438	2.415	2 × 2.0046(3) 2 × 1.9704(8) 2 × 2.0144(8)	1.996	2 × 96.33 2 × 90.6 2 × 91.5	14.5	19	16.75
Er	2.260(1) 2.229(1) 2 × 2.1923(9) 2 × 2.6629(8) 2 × 2.5301(9)	2.407	2.404	2 × 2.0034(3) 2 × 2.0104(9) 2 × 2.0653(9)	2.026	2 × 91.68 2 × 92.43 2 × 90.21	19.5	19	19.25

[a] O^{2-} ionic radii = 1.26 Å.
[b] Ionic radii sum (Fe^{3+}/V^{3+})–O^{2-} = 2.04 Å (as Shannon–Prewitt Ionic radii sum).

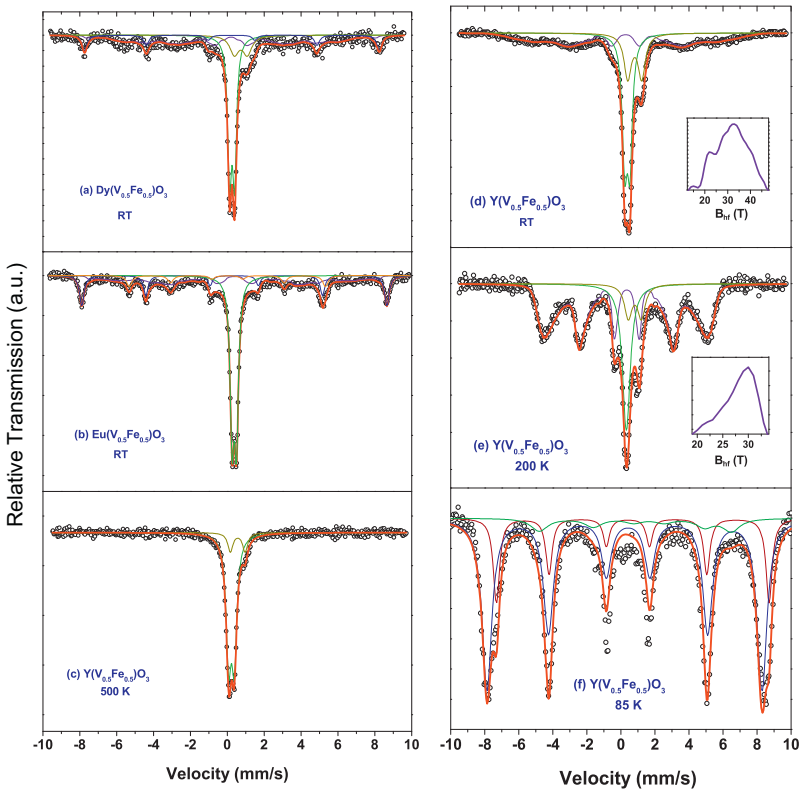

Fig. 3. (a) and (b) Mössbauer spectra for $DyV_{0.5}Fe_{0.5}O_3$ and $EuV_{0.5}Fe_{0.5}O_3$ samples, taken at RT; (c)–(f) $YV_{0.5}Fe_{0.5}O_3$ Mössbauer spectra taken at different temperatures; the inserts represent the hyperfine magnetic field distributions. Mössbauer of the rest of compounds taken at RT are available as supplementary information. (▬) Full theoretical spectra; (▬) Doublet 1; (▬) Doublet 2; (▬) α-Fe sextet; (▬) hyperfine magnetic field distribution; (▬) perovskite (P) sextet (RT); (▬) perovskite (P) Sextet 1 (LT); (▬) perovskite (P) Sextet 2 (LT); (▬) perovskite (P) Sextet 3 (LT). (For interpretation of the references to color in this figure legend, the reader is referred to the web version of this article.)

accepted that the variation in electronegativity of the anion explains the behavior of the IS for these compounds. Evidently, these perovskites contain oxygen, not tellurium, selenium or sulfur, and, according to the Fe^{2+} subspectral areas, oxygen vacancies too. By the criterion of local electronic neutrality, the Fe^{2+} species and vacancies much probably are neighbors (as a pair defect, similar to the Roth complexes) and one could say that each vacancy is part of an anion deficient octahedra or, in other words, belongs, together with five O^{2-}, to a divalent iron cation. That is why the determined IS values are more consistent with penta-coordinated species. Alternatively, we could explain the IS values attributing an "effective" electronegativity to the vacancies, which should be lower than that for oxygen since the capability for receiving electrons would be – if any – lower for a vacancy. Certainly, the IS for the Fe^{2+} must, in each compound, reflect an average effect of the cation neighborhood. The hyperfine parameters table shows that the medium value is ~0.86 mm/s, i.e., similar to that in FeS.

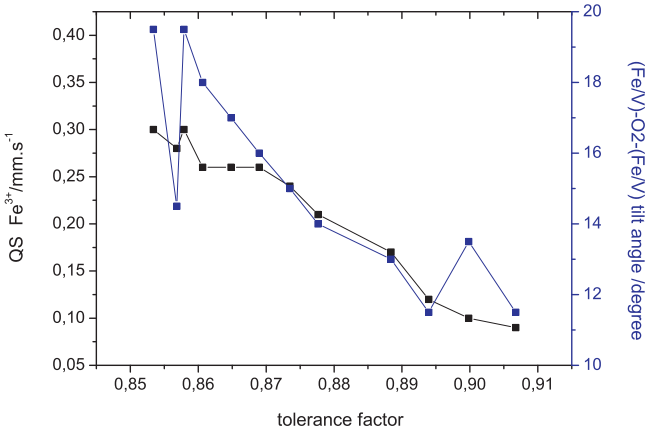

Fig. 4. Tilt angle (Fe/V)–O2–(Fe/V) (in blue) and quadrupolar interaction (QS) (in black), both plotted as a function of Goldschmidt Tolerance factor.

The sextet and the B_{hf} Dist. consistently present similar values for IS and QS and an obvious difference regarding the hyperfine magnetic fields: B_{hf} Dist. has average values between 27.0 T and 39.0 T and the sextet invariably had more than 50.0 T.

In our opinion, the simultaneous presence at RT of a magnetic fraction with a paramagnetic fraction of the same (perovskite) phase may also be responsible (besides the local disordered distribution of iron and vanadium in the octahedral sites, pointed out above) for systems (whatever the Series) transiting between an ordered state (lower temperatures) and a not ordered state (higher temperatures). To some extent, this was not unexpected since ordinary orthoferrites are, in general, magnetically ordered at RT (see in Table 2 the B_{hf} values for these compounds) while the orthovanadates are not [20,29–32].

In order to gain some insight into the situation, we have Mössbauer characterized some samples above and below RT. Fig. 3c–f presents the obtained 500 K, 300 K, 200 K and 85 K spectra for the $YV_{0.5}Fe_{0.5}O_3$ sample. As expected, the magnetic contribution virtually disappeared at 200° above RT whereas two doublets belonging to different valences (i.e., Fe^{3+} and Fe^{2+}) were again found for this compound (in fact, for any other compound belonging to Series II). At the same higher temperature, spectra corresponding to Series I reveal, as before, only one doublet (Fe^{3+}) (spectra not shown).

At 200 K, the magnetic split is more defined, as a result of an increase in the magnetic order of the transition metal sublattice. Finally, at 85 K the spectrum consists of three discrete sextets.

Table 4
Hyperfine parameters and subspectral areas for the $LnV_{0.5}Fe_{0.5}O_3$ perovskites (IS = isomer shift; QS = quadrupole splitting; B_{hf} = hyperfine magnetic field; Γ = linewidth).

Sample	Site/component	IS (mm/s)	QS (mm/s)	B_{hf}[a] (T)	Γ (mm/s)	Area (%)
$LaV_{0.5}Fe_{0.5}O_3$	Doublet 1 (Fe^{3+})	0.39	0.09	–	0.28	23.7
	Doublet 2 (Fe^{2+})	0.91	0.93	–	0.88	10.1
	Dist. B_{hf}	0.39	0.0	31.1	0.27[b]	66.2
	P Sextet	–	–	–	–	0.0
$CeV_{0.5}Fe_{0.5}O_3$	Doublet 1 (Fe^{3+})	0.39	0.10	–	0.27	18.8
	Doublet 2 (Fe^{2+})	0.91	0.70	–	0.75	13.6
	Dist. B_{hf}	0.40	0.10	38.9	0.27[b]	63.4
	P Sextet	0.38	0.0	52.0	0.27	4.2
$PrV_{0.5}Fe_{0.5}O_3$	Doublet 1 (Fe^{3+})	0.38	0.12	–	0.28	34.3
	Dist. B_{hf}	0.41	0.02	33.9	0.27[b]	58.0
	P Sextet	0.38	−0.02	51.9	0.29	7.7
	α-Fe	–	–	–	–	–
$NdV_{0.5}Fe_{0.5}O_3$	Doublet 1 (Fe^{3+})	0.38	0.17	–	0.27	34.4
	Dist. B_{hf}	0.39	−0.06	31.7	0.27[b]	51.2
	P Sextet	0.37	0.0	51.0	0.34	11.3
	α-Fe	0.0[b]	0.0[b]	33.0[b]	0.30[b]	3.1
$SmV_{0.5}Fe_{0.5}O_3$	Doublet 1 (Fe^{3+})	0.38	0.21	–	0.29	41.3
	Dist. B_{hf}	0.40	−0.03	32.6	0.27[b]	34.4
	P Sextet	0.37	−0.12	50.4	0.36	18.4
	α-Fe	0.0[b]	0.0[b]	33.0[b]	0.30[b]	5.9
$EuV_{0.5}Fe_{0.5}O_3$	Doublet 1 (Fe^{3+})	0.38	0.24	–	0.27	43.2
	Dist. B_{hf}	0.38	−0.04	34.7	0.27[b]	28.8
	P Sextet	0.38	0.01	51.3	0.30	19.6
	α-Fe	0.0[b]	0.0[b]	33.0[b]	0.35[b]	8.4
$GdV_{0.5}Fe_{0.5}O_3$	Doublet 1 (Fe^{3+})	0.38	0.26	–	0.27	37.1
	Dist. B_{hf}	0.35	−0.07	34.5	0.27[b]	41.8
	P Sextet	0.36	0.05	51.1	0.38	15.6
	α-Fe	0.0[b]	0.0[b]	33.0[b]	0.35[b]	5.5
$TbV_{0.5}Fe_{0.5}O_3$	Doublet 1 (Fe^{3+})	0.37	0.26	–	0.27	44.3
	Doublet 2 (Fe^{2+})	0.90	0.71	–	0.52	15.4
	Dist. B_{hf}	0.39	−0.03	30.8	0.27[b]	32.7
	P Sextet	0.38	0.07	49.7	0.27	7.6
$DyV_{0.5}Fe_{0.5}O_3$	Doublet 1 (Fe^{3+})	0.37	0.26	–	0.27	42.5
	Doublet 2 (Fe^{2+})	0.89	0.72	–	0.53	12.2
	Dist. B_{hf}	0.31	0.0	32.0	0.27[b]	33.2
	P Sextet	0.35	0.02	49.6	0.33	12.1
$YV_{0.5}Fe_{0.5}O_3$						
85 K	P Sextet 1 (Fe^{3+})	0.48	−0.09	49.5	0.65	68.7
	P Sextet 2 (Fe^{3+})	0.48	−0.09	51.7	0.43	25.0
	P Sextet 3 (Fe^{2+})	1.05	−0.80	35.0	0.90	6.3
200 K	Doublet 1 (Fe^{3+})	0.32	0.00	–	0.56	24.1
	Doublet 2 (Fe^{2+})	0.82	0.77	–	0.54	10.4
	Dist. B_{hf}	0.32	−0.05	27.1	0.27[b]	65.5
300 K	Doublet 1 (Fe^{3+})	0.38	0.30	–	0.35	41.4
	Doublet 2 (Fe^{2+})	0.81	0.82	–	0.51	21.9
	Dist. B_{hf}	0.26	−0.02	31.4	0.27[b]	36.7
	P Sextet	–	–	–	–	0.0
500 K	Doublet 1 (Fe^{3+})	0.22	0.30	–	0.33	86.2
	Doublet 2 (Fe^{2+})	0.56	0.80	–	0.33	13.8
$HoV_{0.5}Fe_{0.5}O_3$	Doublet 1 (Fe^{3+})	0.37	0.28	–	0.27	35.7
	Doublet 2 (Fe^{2+})	0.79	0.70	–	0.66	26.0
	Dist. B_{hf}	0.38	0.09	35.7	0.27[b]	38.3
	P Sextet	–	–	–	–	0.0
$ErV_{0.5}Fe_{0.5}O_3$	Doublet 1 (Fe^{3+})	0.37	0.30	–	0.27	45.7
	Doublet 2 (Fe^{2+})	0.84	0.73	–	0.76	19.9
	Dist. B_{hf}	0.45	0.07	32.4	0.27[b]	34.4
	P Sextet	–	–	–	–	0.0

[a] Average value, in case of distribution.
[b] Value fixed in the fitting procedure.

Actually, all samples recurrently showed the same hyperfine pattern (i.e., three or two discrete sextets, depending on the Series) at this lower temperature (<100 K), whereas the ternary orthoferrites (i.e., $LnFeO_3$) usually show only one sextet, even for T > RT [28,32]. The occurrence of ferric cations in two magnetically and/or crystallographically different sites suggests that a phase transition takes place when lowering the temperature. Here, it is worth remembering that orbital ordering (oo) together with a first order structural transition (i.e., from *Pbnm* without oo to monoclinic $P2_1/b11$ (G-type oo) and at lower temperatures to orthorhombic *Pbnm* (C-type oo) or to a mixture of G-type oo and C-type oo, depending on the lanthanide) are commonly observed for "pure" orthovanadates [10,30,31]. If we consider that the oo is also observed in these orthoferrivanadates, it is reasonable to

assume that the simultaneous presence of both crystallographic phases (a mixture of G-type oo and C-type oo) is plausible – considering a state of partial transformation at low temperatures, in which case the Mössbauer spectra would show two different magnetic components.

Preliminary magnetic measurements (not shown here) have revealed that each $LnV_{0.5}Fe_{0.5}O_3$ system constitutes a complex universe of magnetic phenomena and deserves to be individually analyzed which is outside the scope of this paper and will be presented in a future publication.

4. Conclusions

Metastable $LnV_{0.5}Fe_{0.5}O_3$ perovskites (Ln = Y, La, Ce, Pr, Nd, Sm, Eu, Gd, Tb, Dy, Ho and Er) were successfully prepared by rapid quenching from the isoconcentrational liquid phase, stabilizing the trivalent vanadium cations. These compounds, baptized orthoferrivanadates, crystallized with the *Pbnm* symmetry, i.e., with the single perovskite structure, in which iron and vanadium cations share the same Wyckoff site 4b without any long range order. There is a change from a pseudo-tetragonal perovskite for La to a highly distorted orthorhombic one as the ionic radii of the Ln decreases, because of the decreasing value of the Goldshmidt Tolerance Factor. Usually, iron is also trivalent in these solid solutions although the presence of divalent iron was observed for the Ln = La, Ce, Tb, Dy, Y, Ho and Er samples. The ferrous cation is attributed to the occurrence of oxygen vacancies, in order to achieve the local electronic neutrality. At room temperature, the quadrupolar splitting of the trivalent paramagnetic Mössbauer component can be used (i.e., under variation of the lanthanide ionic radius) as an indirect measure for the Goldshmidt tolerance factor of the $LnV_{0.5}Fe_{0.5}O_3$ perovskites. All these orthoferrivanadates are weakly magnetically ordered at room temperature but become paramagnetic at about 200° above RT. Close to or below 100 K, the orthoferrivanadates undergo a crystallographic phase transformation, probably due to orbital ordering of the V^{3+} cations, originating two different magnetic iron sites.

Supplementary information

Structural information derived from the crystal structure refinement of $LnV_{0.5}Fe_{0.5}O_3$ Perovskites (Ln = Y, La, Ce, Pr, Nd, Sm, Eu, Gd, Tb, Dy, Ho and Er) has been deposited at the ICSD Fachinformationszentrum Karlsruhe (FIZ) (CrysDATA@FIZ.Karlsruhe.DE) with ICSD file numbers: $Ce(V_{1/2}Fe_{1/2})O_3$: **423788**; $Dy(V_{1/2}Fe_{1/2})O_3$: **423789**; $Er(V_{1/2}Fe_{1/2})O_3$: **423790**; $Eu(V_{1/2}Fe_{1/2})O_3$: **423791**; $Gd(V_{1/2}Fe_{1/2})O_3$: **423792**; $Ho(V_{1/2}Fe_{1/2})O_3$: **423793**; $La(V_{1/2}Fe_{1/2})O_3$: **423794**; $Pr(V_{1/2}Fe_{1/2})O_3$: **423795**; $Nd(V_{1/2}Fe_{1/2})O_3$: **423796**; $Sm(V_{1/2}Fe_{1/2})O_3$: **423797**; $Tb(V_{1/2}Fe_{1/2})O_3$: **423798**; $Y(V_{1/2}Fe_{1/2})O_3$: **423799**. Refined Mössbauer spectra at RT for those compounds not shown in this article are available as supplementary information.

Acknowledgments

The authors would like to thank CONICET and CNPq for the CIAM collaboration project. R.E. Carbonio also thanks FONCYT, CONICET and SECYT-UNC for financial support. F.F. Ivashita and V. Biondo also thank CAPES for scholarships.

Appendix A. Supplementary data

Supplementary data associated with this article can be found, in the online version, at http://dx.doi.org/10.1016/j.materresbull.2012.05.055.

References

[1] W.P. Wolf, J. Appl. Phys. 40 (1969) 1061.
[2] V.V. Kharton, A.A. Yaremchenko, A.V. Kovalevsky, A.P. Viskup, E.N. Naumovich, P.F. Kerko, J. Membr. Sci. 163 (1999) 307.
[3] D. Kuscer, M. Hrovat, J. Holc, S. Bernik, D. Kolar, J. Power Sources 61 (1996) 161.
[4] S. Tzong Shen, H. Shan Weng, Ind. Eng. Chem. Res. 37 (1998) 2654.
[5] E. Traversa, S. Matsushima, G. Okada, Y. Sadaoka, Y. Sakai, K. Watanabe, Sens. Actuators B 25 (1995) 661.
[6] M. Mitsuoka, A. Otofuji, T. Arakawa, Sens. Actuators B 9 (1992) 205.
[7] M.C. Carotta, M.A. Butturi, G. Martinelli, Y. Sadaoka, P. Nunziante, E. Traversa, Sens. Actuators B 44 (1997) 590.
[8] D.S. Schmool, N. Keller, M. Guyot, R. Krishnan, M. Tessier, J. Appl. Phys. 86 (1999) 5712.
[9] H. Sakakima, M. Satomi, E. Hirota, H. Adachi, IEEE Trans. Magn. 35 (1999) 2958.
[10] M.H. Sage, G.R. Blake, C. Marquina, T.T.M. Palstra, Phys. Rev. B 76 (2007) 195102.
[11] S. Miyasaka, Y. Okimoto, M. Iwama, Y. Tokura, Phys. Rev. B 68 (2003) 100406.
[12] P. Schiffer, A.P. Ramirez, W. Bao, S.-W Cheong, Phys. Rev. Lett. 18 (1995) 3336.
[13] S. Jin, T.H. Tiefel, M. McCormack, R.A. Fastnacht, R. Ramesh, L.H. Chen, Science 264 (1994) 413.
[14] J. Androulakis, N. Katsarakis, J. Giapintyakis, Solid State Commun. 124 (2002) 77.
[15] M.H. Sage, G.R. Blake, T.T.M. Palstra, Phys. Rev. B 77 (2008) 155121.
[16] T. Shin-ike, T. Sakai, G. Adachi, J. Shiokawa, Mater. Res. Bull. 13 (1978) 1105.
[17] M. Gateshki, L. Suescun, S. Kolesnik, J. Mais, B. Dabrowski, J. Solid State Chem. 184 (2011) 2374.
[18] J. Rodríguez-Carvajal, Physica B 192 (1993) 55.
[19] R. Sen, S. Das, K. Das, Metall. Mater. Trans. A 42 (2011) 1409–1417.
[20] J.B. Goodenough, Rep. Prog. Phys. 67 (2004) 1915.
[21] I.D. Brown, in: M. O'Keeffe, A. Navrotsky (Eds.), Structure and Bonding in Crystals, vol. 1, Academic Press, New York, 1981.
[22] G.J. McCarthy, C.A. Sipe, K.E. McIlvried, Mater. Res. Bull. 9 (1974) 1279–1284.
[23] M.J. Martínez-Lope, J.A. Alonso, M. Retuerto, M.T. Fernández-Díaz, Inorg. Chem. 47 (2008) 2634–2640.
[24] M. Marezio, J.P. Remeika, P.D. Dernier, Acta Crystallogr. B 26 (1970) 2008–2022.
[25] R.D. Shannon, C.T. Prewitt, Acta Crystallogr. B 26 (1970) 1046–1048.
[26] I.D. Brown, R.D. Shannon, Acta Crystallogr. A 29 (1973) 266–282.
[27] K. Robinson, G.V. Gibbs, P.H. Ribbe, Science 172 (1971) 567–570.
[28] N.E. Erickson, in: R.F. Gould (Ed.), The Mössbauer Effect and its Application in Chemistry, American Chemical Society, 1967.
[29] M. Eibschütz, S. Shtrikman, D. Treves, Phys. Rev. 156 (1967) 562.
[30] T. Sakai, G. Adachi, J. Shiokawa, J. Appl. Phys. 48 (1977) 379.
[31] D. Treves, J. Appl. Phys. 36 (1965) 1033.
[32] S. Acharya, A.K. Deb, D. Das, P.K. Chakrabarti, Mater. Lett. 65 (2011) 1280–1282.